Electronic Supplementary Information

Layer-by-layer fabrication of fluorescent microspheres using micelles as the spacer: simultaneously realizing fluorescence enhancement and introduction of bioconjugation sites

Lijuan Sun, Tian Qiu, Jiangxin Liu, Ke Miao, Youliang Zhao* and Li-Juan Fan*
State and Local Joint Engineering Laboratory for Novel Functional Polymeric Materials, Jiangsu Key Laboratory of Advanced Functional Polymer Design and Application, College of Chemistry, Chemical Engineering and Materials Science, Soochow University, Suzhou 215123, Jiangsu, P. R. China
Emails: ylzhao@suda.edu.cn, ljfan@suda.edu.cn

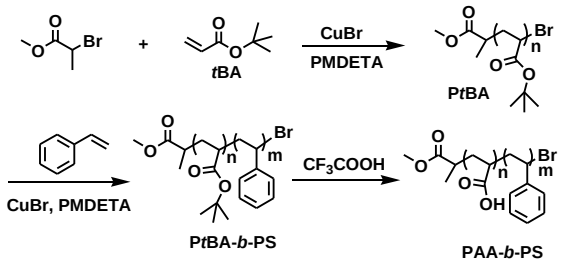

Scheme S1. The synthetic route of PAA-*b*-PS

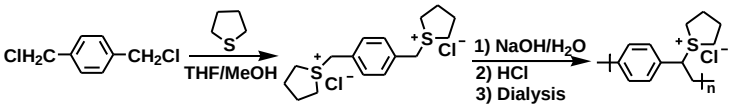

Scheme S2. The synthetic route of pre-PPV.

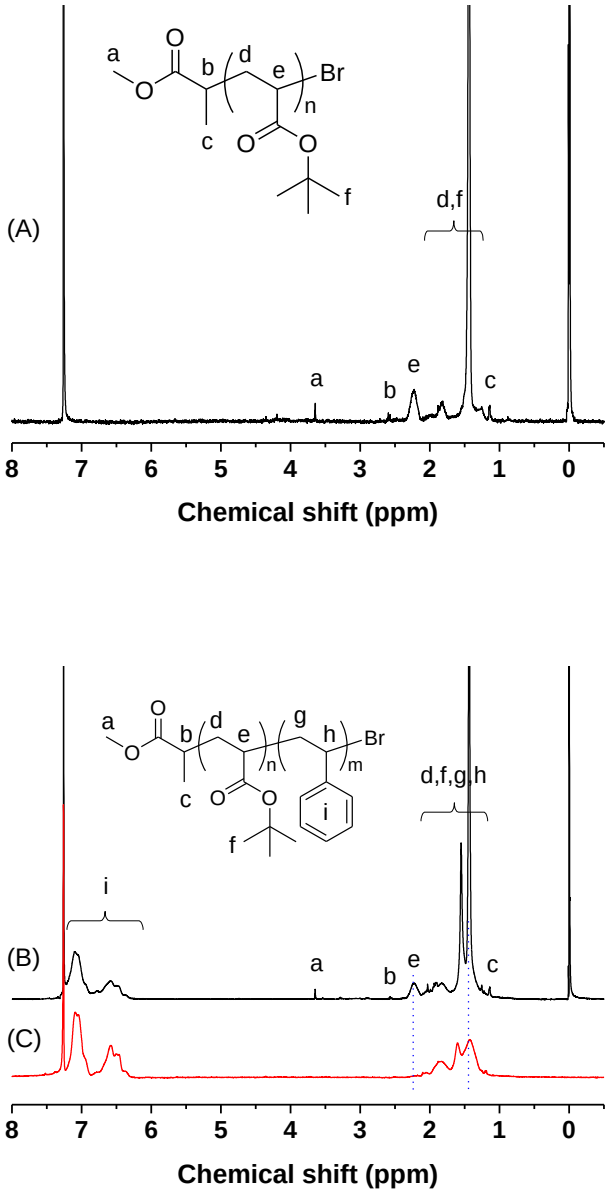

Fig. S1. ^{1}H NMR spectra of P*t*BA (A), PtBA-*b*-PS (B), and PS-*b*-PAA (C) recorded in $CDCl_3$.

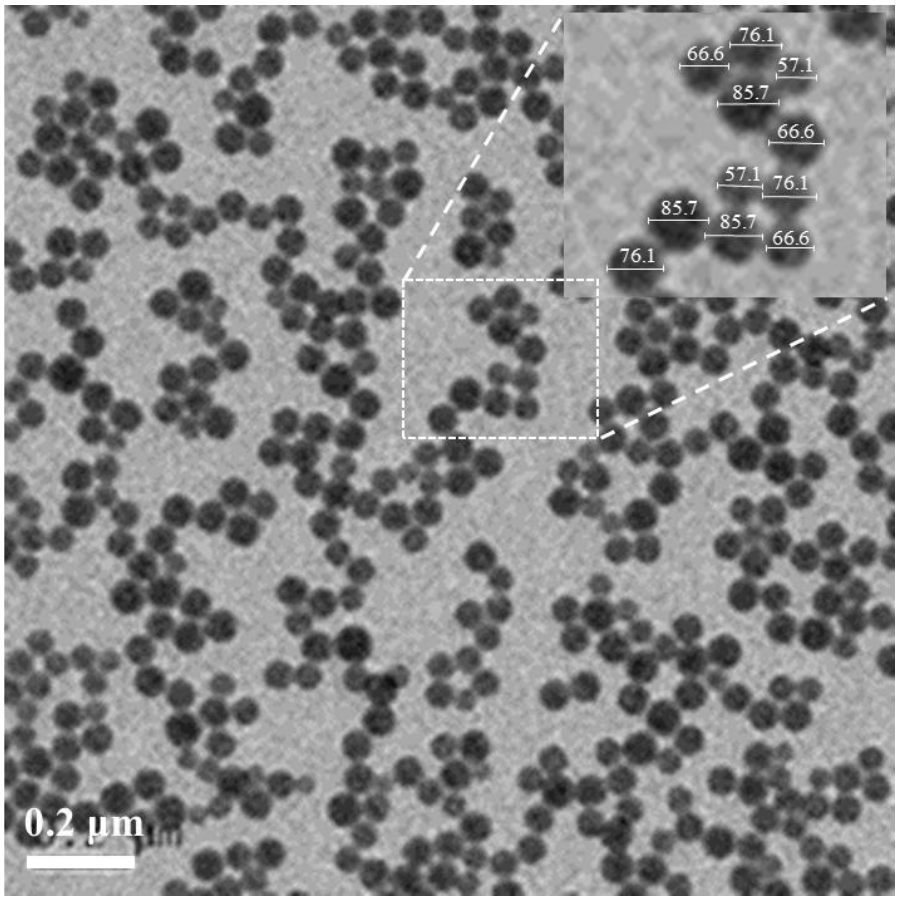

Fig. S2. Size measurement for the TEM image of micelles. All clear and complete micelles (327 micelles) were measured. Inset shows the enlarge part of such measurement carried out on the micelles in a specific region.

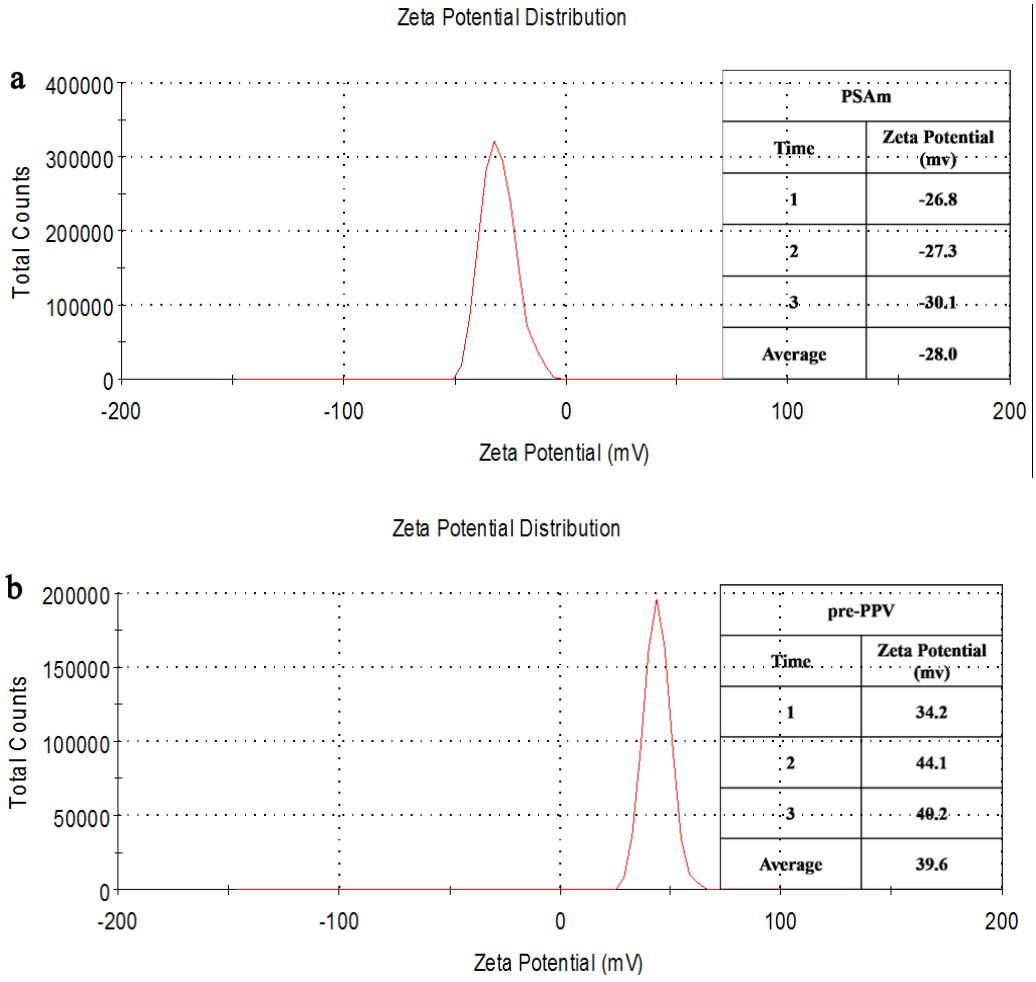

Fig. S3. The Zeta potential curves for PSAm (a) and pre-PPV (b) (only one curve is shown for each as representative); and the insets shown the values from three measurements for each, and the average value from 3 measurements of Zeta potentials are -28.0 mV and 39.6 mV for PSAm and pre-PPV, respectively.

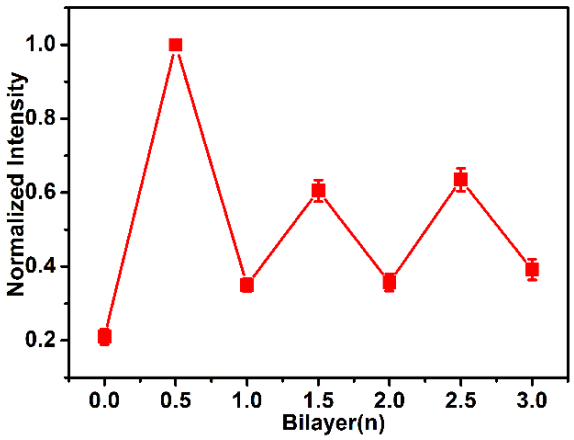

Fig. S4. Emission intensities from flow cytometry (excited at 488 nm, emission received from 527 ± 16 nm channel) for SPSDVB-(PPV/PAA)$_n$. The error bars shown are based on the calculated standard deviations from the average value of three measurements from flow cytometry with spheres having the same composition but from different batches; for each measurement, the intensity was normalized with respect to the intensity of SPSDVB-PPV spheres to make the data from different measurements comparable. It is to be noted that when n is 0.5, 1.5 and 2.5, pre-PPV is the outermost layer; and when n is 1, 2 and 3, PAA is the outermost layer.

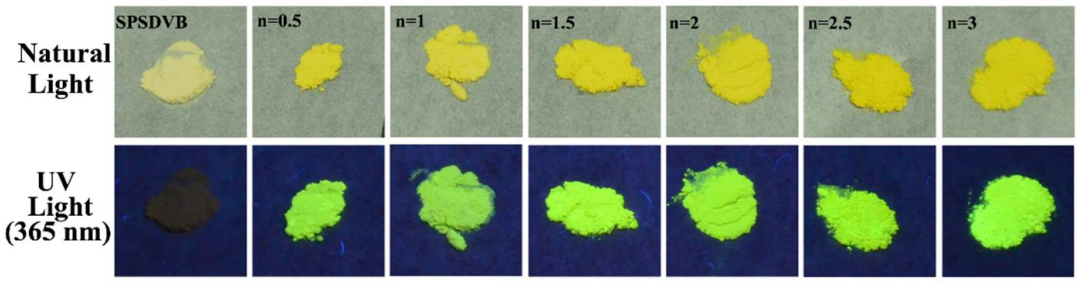

Fig. S5. The digital photographs of SPSDVB and SPSDVB-(PPV/PSAm)$_n$ solid microspheres under natural light and UV light (365 nm).

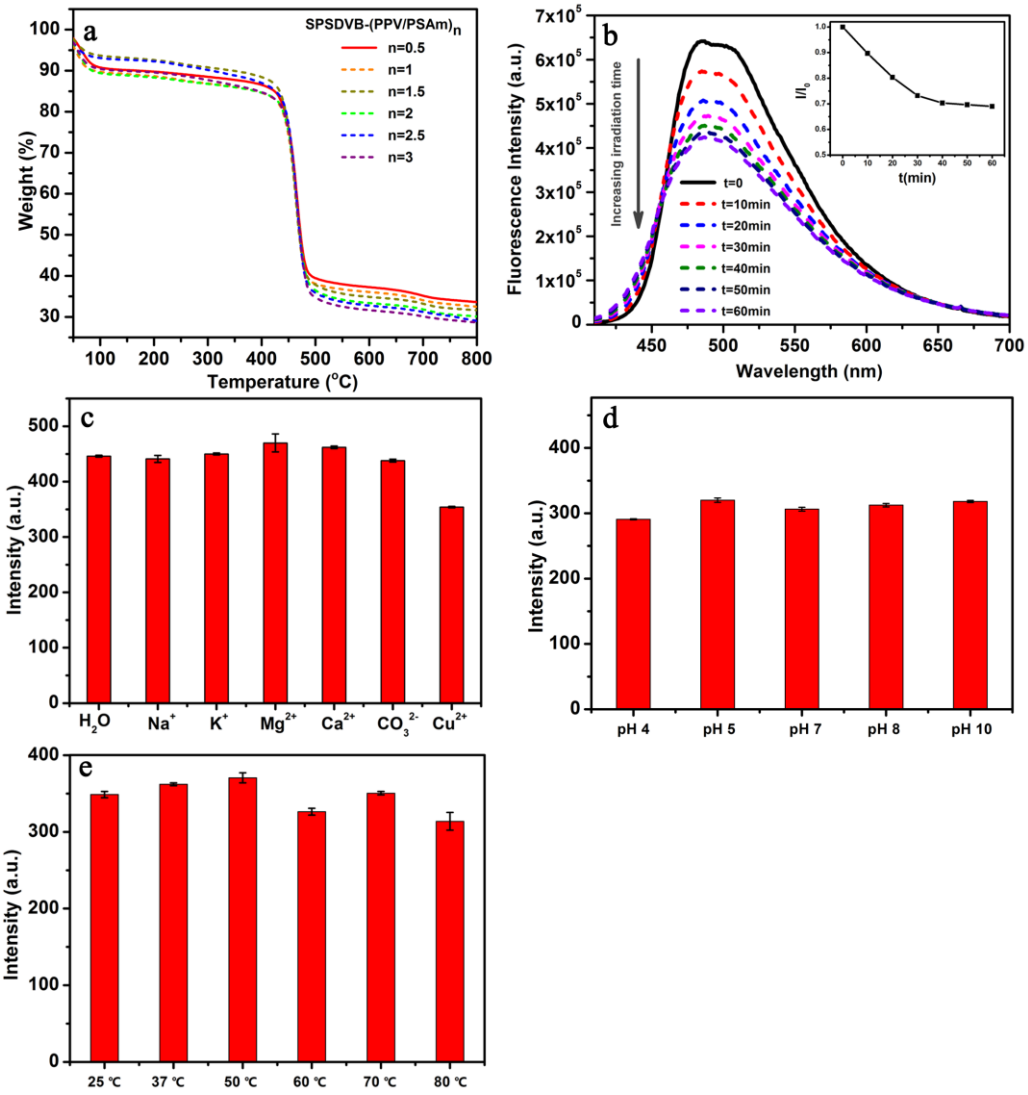

Fig. S6. Thermogravimetric analysis of SPSDVB-(PPV/PSAm)$_n$ microspheres(a); The emission spectra for SPSDVB-(PPV/PSAm)$_3$ after irradiation for various times (b); The average intensity at the emission maxima (from three measurements) of SPSDVB-(PPV/PSAm)$_3$ microspheres: mixed with different ions (0.01M) (c), under different pH environment (d) and under different temperatures (e). The excitation was set at 385 nm.

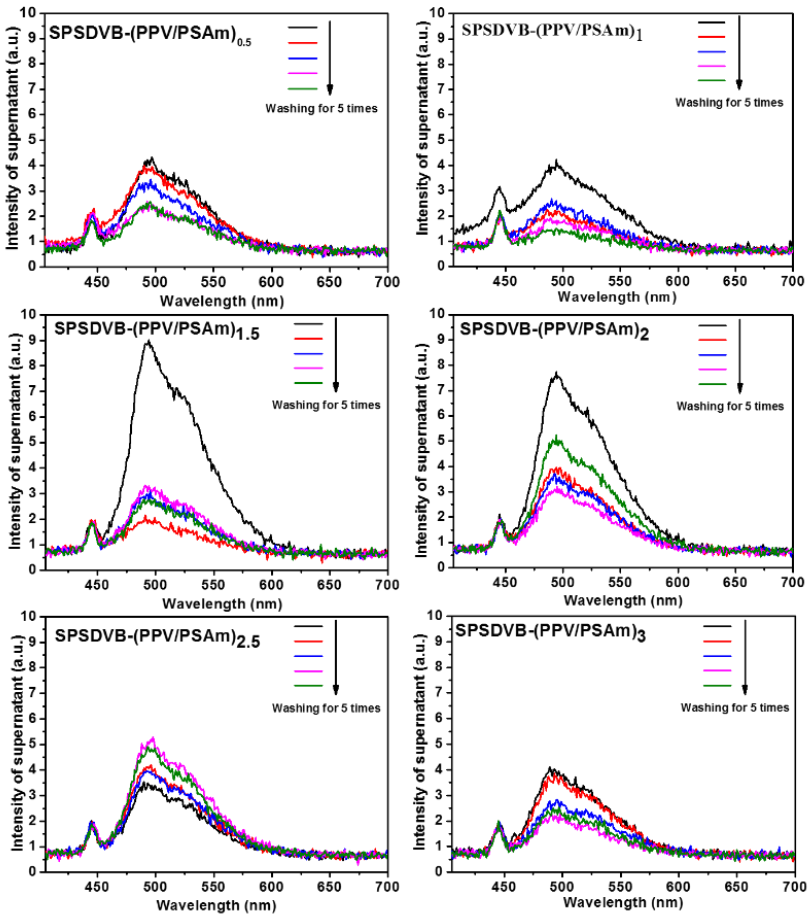

Fig. S7. The emission spectra of the supernatant obtained during the process of washing SPSDVB-(PPV/PSAm)$_n$ for 5 times.

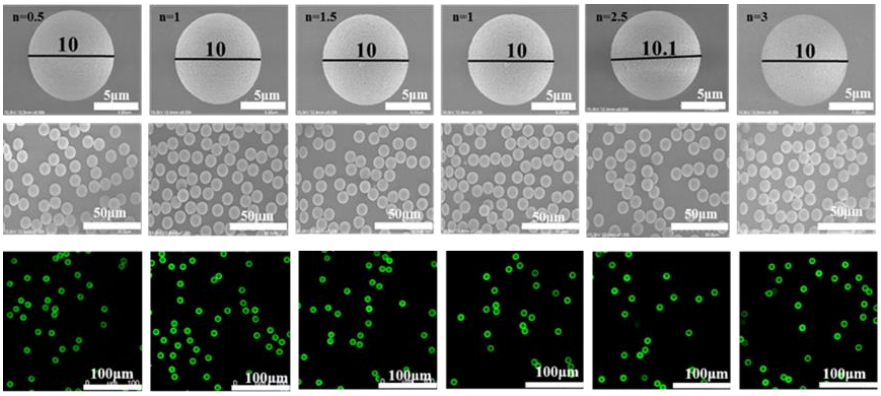

Fig. S8. SEM images of the SPSDVB-(PPV/PSAm)$_n$ microspheres (top) and the confocal images were obtained by receiving emission at the 420−650 nm channel with excitation at 405 nm of the SPSDVB-(PPV/PSAm)$_n$ microspheres (bottom).

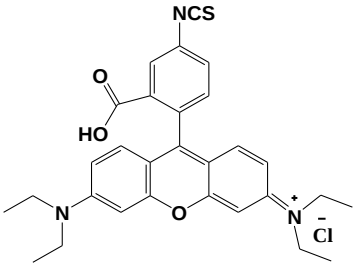

Fig. S9. The chemical structure of Rhodamine B isothiocyanate (RBITC).

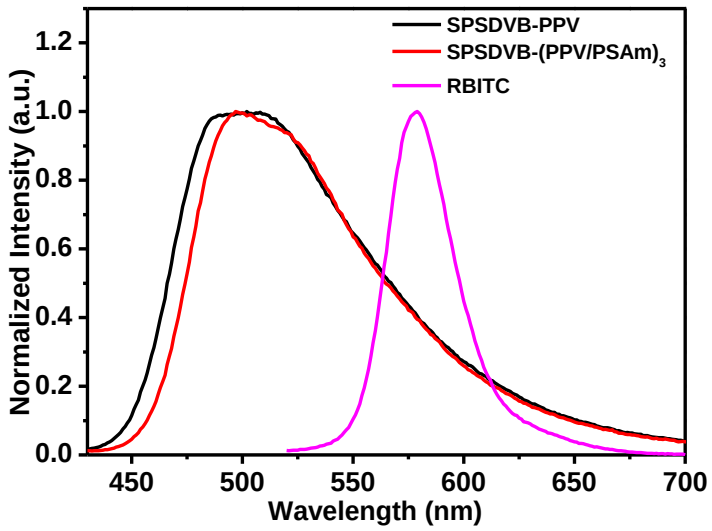

Fig. S10. Normalized fluorescence spectra of SPSDVB-PPV, SPSDVB-$(PPV/PSAm)_3$ and RBITC.

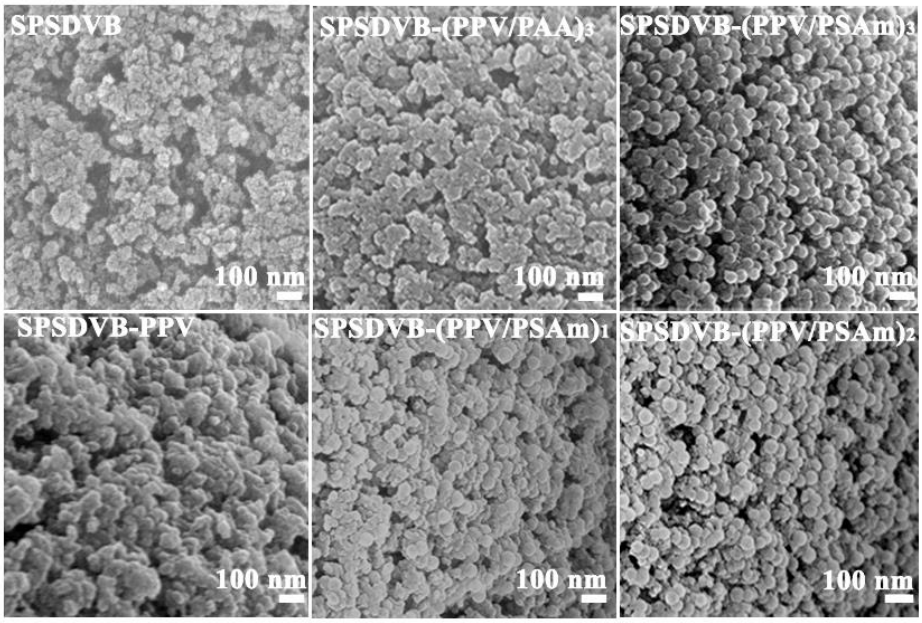

Fig. S11. The enlarged SEM images of the surfaces of SPSDVB, SPSDVB-$(PPV/PAA)_3$, SPSDVB-$(PPV/PSAm)_3$, SPSDVB-PPV, SPSDVB-$(PPV/PSAm)_1$ and SPSDVB-$(PPV/PSAm)_2$ microspheres.

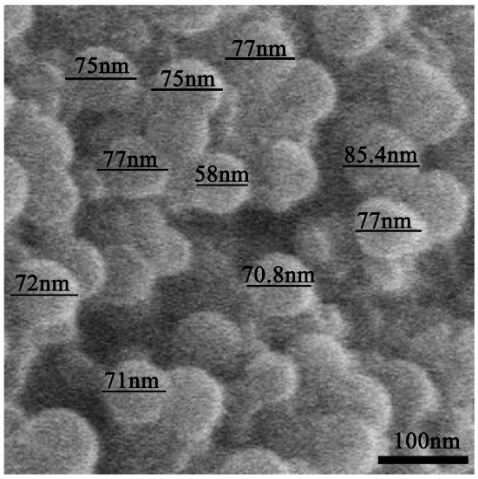

Fig. S12. Particle size measurement of the nanoparticles appeared on the surface of SPSDVB-(PPV/PSAm)$_3$ in SEM image, using 10 particles as the representative.